Microscopic view of the role of repeated polytypism in self-organization of hierarchical nanostructures

Ming Liu,[1] Guo-Bin Ma,[1] Xiang Xiong,[1] Zhao-Wu Wang,[1] Ru-Wen Peng,[1] Jian-Guo Zheng,[2] Da-Jun Shu,[1] Zhenyu Zhang,[3] and Mu Wang[1,*]

[1]*National Laboratory of Solid State Microstructures and Department of Physics, Nanjing University, Nanjing 210093, China*

[2]*Laboratory for Electron and X-ray Instrumentation, Calit2, University of California, Irvine, California 92697, USA*

[3]*International Center for Quantum Design and Functional Materials, Hefei National Laboratory for Physical Science at Microscale, University of Science and Technology of China, Hefei 230026, China*

In this article we report our experimental observations that the repeated polytypism of wurtzite (WZ) and zinc-blende (ZB) phases induced by the fluctuation of the density of stacking faults can lead to the self-organized formation of ZnO hierarchical nanostructures characterized by a hexagonal central trunk decorated with thin blades. The blades epitaxially nucleate on the ZB stripes assisted by the reentrant corners at the ZB-WZ interfaces. Consequently, the blades keep a fixed angle with respect to the central trunk and resemble two sets of mutually intercalated propellers, each set possessing its own threefold rotational symmetry and being rotated for 60° with respect to each other. We also study the optical properties of such novel structures, and show through numerical simulations that the blades provide the essential boundary conditions to establish the resonant electromagnetic responses in the hierarchical nanostructures.

PACS number(s): 81.10.−h, 61.72.−y, 64.75.Yz, 68.70.+w

I. INTRODUCTION

Understanding the underlying formation mechanisms, controlling the morphologies, exploring their emergent properties, as well as exploiting their technological potentials are the central aspects of materials discovery of novel nanostructures.[1–5] As an important class of specific materials examples, ZnO semiconductor nanorods typically possess hexagonal cross sections, and can be exploited for development of a rich variety of new generation optoelectronic devices. In particular, recent studies have shown that such nanorods can be applied to develop polariton lasers,[6–10] where the coupling of resonant modes and free excitons sensitively depends on the geometry of the cross sections. It is therefore essential to gain precise control of the nanostructural morphology. However, despite decades of enduring research efforts, the underlying microscopic mechanisms for the formation of such quasi-one-dimensional (quasi-1D) nanostructures remain largely unexplored, especially with regard to quasi-1D hierarchical nanostructures. Most previous reports ascribe the formation of hierarchical nanostructures to the contributions of a given catalyst within the vapor-liquid-solid (VLS) mechanism.[11,12] In the VLS process, a catalytic liquid droplet on top of a nanowire adsorbs ambient vapor atoms, and subsequently nucleates crystals on liquid-solid interface.

In nanocrystalization microscopic defects such as dislocations are usually absent.[13] On the other hand, it has been predicted decades ago that screw dislocations in an ultrathin crystalline rod may induce a torque, lead to an elastic twist of the crystalline lattice, and eventually form a chiral pattern if one end of the rod is free to rotate.[14] However, such an effect has not been experimentally observed until very recently, where a dislocation within the nanowire leads to a chiral hierarchical structure.[15,16] Stacking fault, a common two-dimensional defect in semiconductor crystallization,[17–19] has so far not been recognized to play any role in generating hierarchical nanostructures.

In this article, we present for the first time the remarkable contribution of stacking-fault-induced repeated polytypism on the formation of a unique hierarchical structure of ZnO nanorods, characterized by a hexagonal central trunk decorated with thin blades. The blades keep a fixed angle with respect to the central trunk, and resemble two sets of mutually intercalated propellers, each set possessing its own threefold rotational symmetry and being rotated for 60° respect to each other. Our detailed structural analysis shows that the blades are epitaxially initiated through reentrant-corner-mediated nucleation. This finding demonstrates a previously unknown example of self-assembly process of hierarchical nanostructures controlled by polytypism, an intriguing new mechanism that may find broader applicability. We also explore the novel optical properties of such hierarchical nanostructures.

II. EXPERIMENTAL AND NUMERICAL METHODS

The hierarchical structures of ZnO are fabricated on silicon (100) substrate by thermo-evaporation method. A horizontal tube furnace is used to grow ZnO nanostructure with ultrapure N_2 as the carrier gas, where the zinc source is pure zinc powder (99.9%) without adding any catalysts. The system is heated to 550 °C at a rate of 25 °C/min and the temperature is kept at 550 °C during the growth process. Trace amount of ultrapure oxygen gas (3 sccm) is introduced into the furnace as the oxygen source. The substrate is placed 10 mm up stream of the zinc powder. To terminate the ZnO growth, the flux of O_2 is cut off first, followed by blowing in large flux of ultrapure N_2 (∼5000 sccm) into the furnace and decreasing

temperature afterwards. A layer of the ZnO structure covers on the whole silicon substrate. The morphology and structures of the hierarchical ZnO structures were characterized with a field-emission scanning electron microscope (FESEM) and high-resolution transmission electron microscope (HRTEM). Cathodoluminescence (CL) spectroscopy was carried out at room temperature with Gatan MonoCL3+ associated with the FESEM.

The interaction of light and the ZnO trunk decorated with periodically distributed, uniformly angled blades was numerically simulated with commercial software based on the finite difference time domain (FDTD) method. The incident light was *z* polarized, and shined normal to the trunk. In the simulation, the boundaries in *x* and *y* directions were set as perfectly matched layer (PML) condition. Periodic boundary condition was applied in the *z* direction of the ZnO trunk and the periodicity of unit cells was set as 0.9 μm. The separation between two adjacent sets of blades within the unit cell (which was rotated for 60° with respect to the axis of the main trunk) was 0.3 μm. Each side of the hexagonal cross section of the main trunk was 0.4 μm. The thickness of each blade was 0.05 μm. The refractive index of ZnO was set as 2.0 in the simulation.

III. RESULTS

A. Microstructures of ZnO nanopropellers

The large view field of the ZnO nanostructures grown on silicon substrate observed with FESEM is shown in Fig. 1. The zoom-in micrographs of the ZnO microstructure with a hexagonal central trunk decorated with flat paddle blades are shown in Fig. 2. Although the blades seem to possess a sixfold symmetry with respect to the central trunk, they in fact belong to two sets of the threefold symmetrical group, each originates from a different section on the hexagonal trunk and has been rotated by 60° with the central trunk as the axis [Fig. 2(b)]. From the same section of the trunk, only three blades develop outwards, keeping a threefold symmetry to the trunk. The neighboring blade either nucleates on the same facet of the hexagonal trunk (and hence in parallel with the existing blade), or nucleates on an adjacent facet that has rotated by 60° around the central trunk. The blades keep a fixed angle with respect to
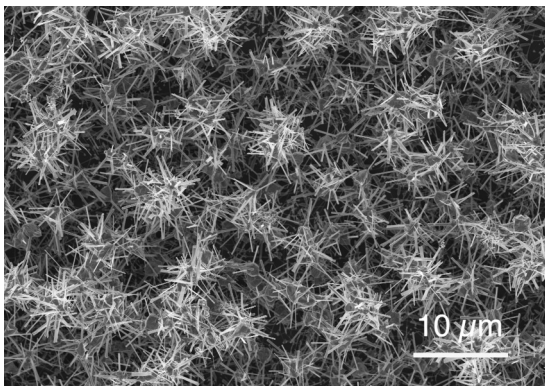

FIG. 1. Large view field of the hierarchical ZnO nanostructures grown on silicon substrate observed with FESEM.
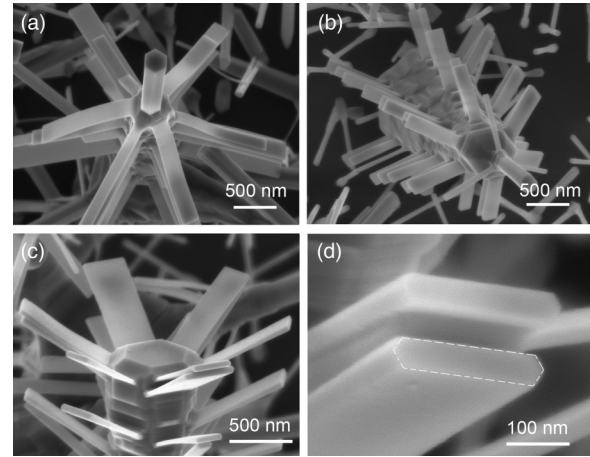

FIG. 2. FESEM micrographs of ZnO hierarchical nanostructures composed of a hexagonal trunk decorated with two sets of mutually intercalated paddle blades, each set with its own threefold rotational symmetry, and being rotated for 60° with respect to each other. (a) Top, (b) side, and (c) bottom views, respectively. (d) High magnification image showing the flat hexagonal cross sections of the blades. The dashed lines in (d) serve as guides to the eye.

the central trunk (Fig. 2), suggesting intrinsic structural origins for the formation of the ZnO propellers.

The HRTEM of the ZnO hierarchical pattern is shown in Fig. 3. It has been well established that in ambient conditions the hexagonal wurtzite (WZ) structure is the most stable polymorph of ZnO and is hence most commonly observed.[20] Yet ZnO may also crystallize into the cubic zinc-blende (ZB) structure.[21–23] Figure 3(a) illustrates a TEM micrograph of the central trunk and propeller blades. It can be identified in Fig. 3(c) that both the trunk and blade are in the WZ phase, whereas immediately adjacent the blade in the main trunk there is a defected ZB region. Region 1 (WZ) is in the side-branching blade and is nearly defect-free; region 3 (WZ) is a part of the main trunk and contains visible stacking faults. Region 2 is a ZB slab with some stacking faults. The side-branching blade roots from the ZB slab in region 2 and develops outward. During the growth both the blade and main trunk are simultaneously thickened, so a conical region (shoulder section) is generated [as marked by the red dashed lines in Fig. 3(b)]. Since the WZ and ZB structures differ merely in stacking sequences of the closely packed atomic planes, the ZB {111} planes are parallel to the WZ {0001}, as indicated by the red lines in Fig. 3(c). In region 2, as marked by the bright yellow lines, the (0001) planes of the blade are approximately parallel to the $(1\bar{1}\bar{1})$ planes of the ZB phase. The angle between the growth direction of the blade and that of the trunk is measured as 104°, very close to the angle between two equivalent ZB {111}, 109.5°.

Microscopically, the WZ structure of ZnO is constructed with closely packed Zn and O layers stacked along the [0001] direction in the sequence of ABABAB [Fig. 3(e)]. Yet sequence ABCBABA or ABCABAB appears when a stacking fault is formed. If stacking fault occurs continuously, the local structure may change from the hexagonal WZ phase to the cubic ZB phase [Fig. 3(e)]. For III-V and II-VI compounds, basal-plane stacking faults are frequently observed due to
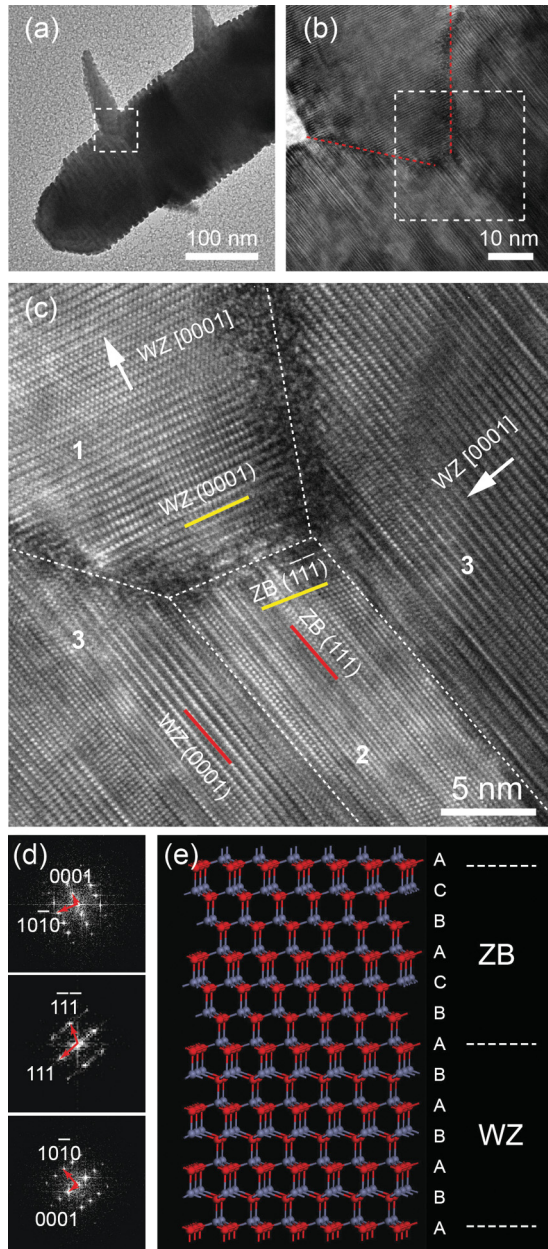
FIG. 3. (Color online) Microstructural analysis of the ZnO propellers composed of a main trunk with layers of paddle blades. (a) Bright field TEM image, with the boxed region further enlarged in (b). (c) HRTEM image of the boxed region in (b). Regions 2 and 3 are on the main trunk and region 1 belongs to the side-branching blade. (d) Fast Fourier transforms (FFTs) for different regions in (c); from top to bottom, the graphs represent the FFTs in regions 1, 2, and 3, respectively. Both the main trunk and the blades are assigned to the WZ structure, with the growth direction along the [0001] (the angle between them is 104°); the main trunk, however, is composed of ZB segments and stacking faults. (d) Atomic structure illustrating the WZ-ZB combination.

their very low formation energies.[24,25] A high concentration of stacking faults changes the structure from WZ to ZB.[24] It is noteworthy that for the scenario that a ZB segment is sandwiched by WZ-structured parts, there exist energetically identical yet crystallographically different stacking sequences,
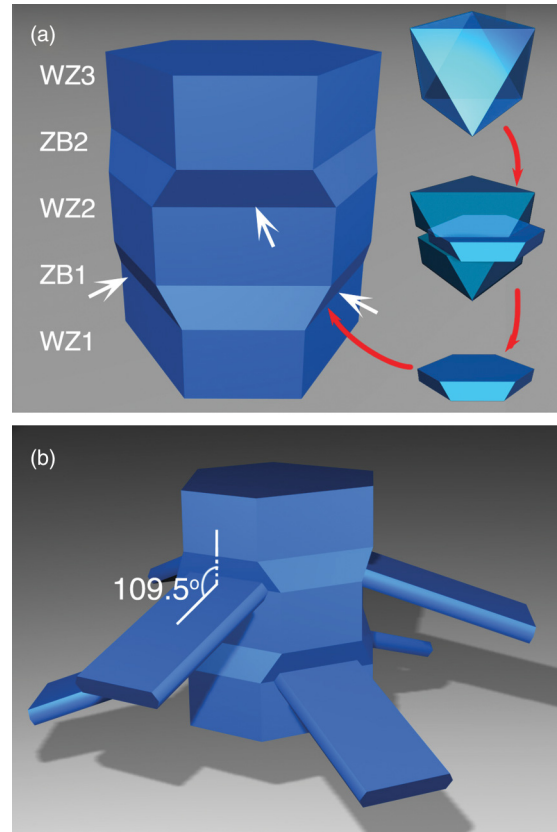

FIG. 4. (Color online) Schematic illustrations of the crystallographic structure of the propellers. (a) The central trunk composed of alternating stackings of WZ and ZB slices. The side surfaces of the WZs are $\{10\bar{1}0\}$ facets, while those of the ZBs are $\{111\}$ facets. ZB1 and ZB2 represent two ZB layers with different stacking sequences and are crystallographically rotated by 60° around the [111] axis. The white arrows indicate the reentrant sites (160.5°) formed by the ZB $\{111\}$ and the underneath WZ $\{10\bar{1}0\}$ surfaces. Curved red arrows illustrate how a ZB segment is truncated from a $\{111\}$ octahedron, where the Zn- and O-terminated surfaces (four for each type) are represented by darker and lighter hues, respectively. For ZnO the growth rate of the Zn-terminated facet is much higher. (b) Schematic for a hierarchical propeller structure generated by epitaxial growth of WZ branches on the Zn-terminated ZB faces from the reentrant sites.

e.g., . . . AB**ABCABC**AB . . . and . . . ABA**CBACBA**BAB . . . , where the underlined bold letters indicate the ZB segments. Topologically these two configurations differ by 60° with the [111] axis. As elucidated in detail below, this feature determines the seemingly sixfold symmetrical blades around the trunk.

B. Growth mechanism of the hierarchical structure

For a ZnO segment with WZ structure, the large flat surface is $\{0001\}$, and the side surfaces of the WZ segment on the trunk are $\{10\bar{1}0\}$,[26] which has been reconfirmed by our HRTEM micrographs. For the ZB structure, the $\{111\}$ planes are the energetically preferred facets. Therefore, a ZB segment is modeled as a truncated $\{111\}$ octahedron [the inset of Fig. 4(a)]. We schematically plot three WZ and two ZB segments, which mimic a section of the central trunk where a structural transformation takes place. The top and side surfaces of the WZ

segments are {0001} and {10$\bar{1}$0} facets, respectively,[26] whereas the surfaces of the ZB structures are all {111}. Consequently a reentrant angle of 160.5° appears at the junction of the side surfaces of the WZ {10$\bar{1}$0} and neighboring ZB {111} planes, where a side-branching blade can be nucleated [Fig. 4(a)]. The experimentally observed bumpy side surface of the central trunk [Fig. 2(b)] is consistent with this configuration.

For nucleation, thermodynamically there exists a critical size of the embryo of a nucleus r^*. Beyond r^* an embryo can survive and develop into a nucleus. As a substrate, the width of the ZB slab should be much larger than the critical size of embryo for nucleation. It follows that this critical slab width will be expressed as

$$W_{ZB}^c \sim r^* = \frac{2\gamma_{sv}\Omega_s}{kT \ln \frac{P}{P_0}},$$

where γ_{sv} is the interfacial energy of the ZnO/vapor interface; Ω_s is the volume of unit cell in the WZ phase; P_0 is the equilibrium pressure and P is the real pressure in vapor growth, k is the Boltzman constant, and T is temperature. By taking the data $\gamma_{sv} = 1.15$ J/m^2, $\Omega_s = 71.35 \times 10^{-30}$ m^3, $T = 823$ K, and P/P_0 is of the order of 100 (Ref. 27), it follows that $W_{ZB}^c \sim 3 \times 10^{-9}$ m. This means that once the ZB slab is thicker than W_{ZB}^c, then the embryo of the blades will be accommodated and developed further. This value is comparable with our TEM observations, where the ZB slab is of the order of several nanometers.

For both configurations of the ZB segment embedded in the WZ trunk, the ZB {111} planes epitaxially grow on WZ {0001}. Therefore, the ZB-WZ interface is an atomically matched coherent interface, and the orientation of ZB1 and ZB2 can be rotated by 60° along the [111] direction [Fig. 4(a)]. At the interface of ZB and WZ segments, {111} of the ZB and {10$\bar{1}$0} of the WZ phases form six reentrant corners. Due to the electric neutralization requirement, each facet is alternatively terminated by O or Zn, as illustrated with a different shade in Fig. 4(a). Among the six reentrant corners, only three possess Zn-terminated ZB {111}. It is well established that the reentrant corner site possesses a lower nucleation barrier and is energetically more favorable for nucleation.[28] It is also known that the fast growing facets of ZnO are the Zn-terminated ones.[12] Consequently, as the main trunk develops along the ZB [111] direction with a Zn-terminated facet, three side-branching blades are nucleated at the reentrant corners with Zn-terminated ZB {111} and further develop downwards to form a propeller pattern [Fig. 4(b)].

It should be emphasized that the blade nucleates from the confined lamella of ZB {111}, so the cross section of the blade is strongly confined and hence has an elongated hexagon pattern [Fig. 2(d)]. Geometrical calculations show that the angle between the blade and the main trunk should be 109.5° [Fig. 4(d)], consistent with our experimental observations (~104°) [Fig. 3(b)]. It is noteworthy that on each segment of the ZB phase there are three Zn-terminated reentrant corners. On the neighboring ZB segments, such as ZB1 and ZB2, the sites with the same type of reentrant corners can be rotated by 60° with the WZ [0001] axis, which eventually leads to the seemingly sixfold symmetry of the blades.
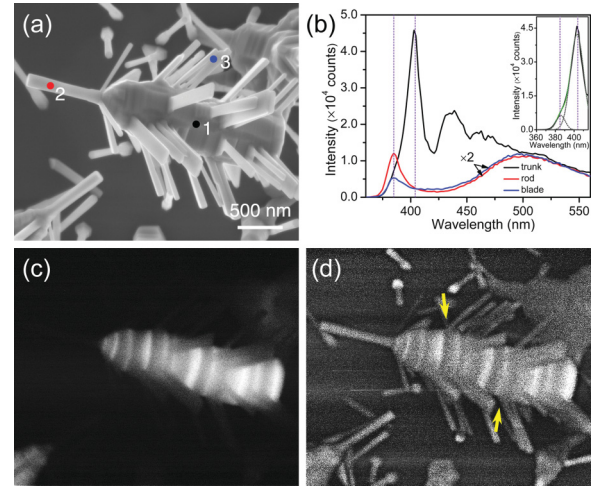

FIG. 5. (Color online) SEM micrograph, CL spectra, and monochromic CL images of the ZnO hierarchical nanostructures. (a) Micrograph of a ZnO propeller. (b) CL spectra recorded at different locations (as schematically marked in A). The vertical dotted lines indicate the positions of wavelengths of 385 and 405 nm. Spectra from the hexagonal prism on top of the trunk and the blade are enlarged by a factor of 2. Inset shows the Gaussian decomposition of the trunk emission peak at around 400 nm. (c) Monochromic CL images obtained with 405-nm emission. (d) The superimposed image of the SEM image. (c) Shows that the blades originate exactly from the intersections of the bright and dark emission bands, as marked by the yellow arrows.

C. Further proof on the growth mechanism: cathodoluminescence studies

In order to verify the above mechanism, we have carried out cathodoluminescence (CL) spectroscopy on the ZnO hierarchical nanostructure. ZnO has intrinsic ultraviolet luminescence around 385 nm, which is conventionally attributed to the recombination of free excitons in the WZ structure.[29] In addition, defect-related blue to green band emissions have been reported.[30] Theoretical calculations of the energy band gap of the ZB-type ZnO indicate that it is approximately 0.1 eV lower than that of the WZ-type ZnO.[25,31] The narrower band gap means a red-shift of the primitive emission of the ZB-type ZnO with respect to that of the WZ type. Accordingly, one would expect to observe luminescence of the ZB-type ZnO around 400–410 nm. Figure 5 shows room temperature CL measurements on the ZnO hierarchical nanostructure. Based on the HRTEM observations, both the thin hexagonal prism on the foreside of the thick central trunk and the flat blades aside of the main trunk are in the WZ phase (Fig. 3), and the thick central trunk possesses ZB lamella embedded in the WZ phase. As illustrated in Fig. 5(b), the blades and the thin perfect hexagonal prism on top of the central trunk are luminescent at 385 nm. On the main trunk, there is a distinct sharp peak centered at 405 nm, together with a minor shoulder at 385 nm [Fig. 5(b)]. With monochromatic imaging at 405 nm, bright strips appear on the trunk [Fig. 5(c)], which are expected to be the locations of ZB lamella. The darker regions between the bright strips are in the WZ phase. Combining monochromatic imaging at 405 nm and the morphology, we conclude that the blades originate
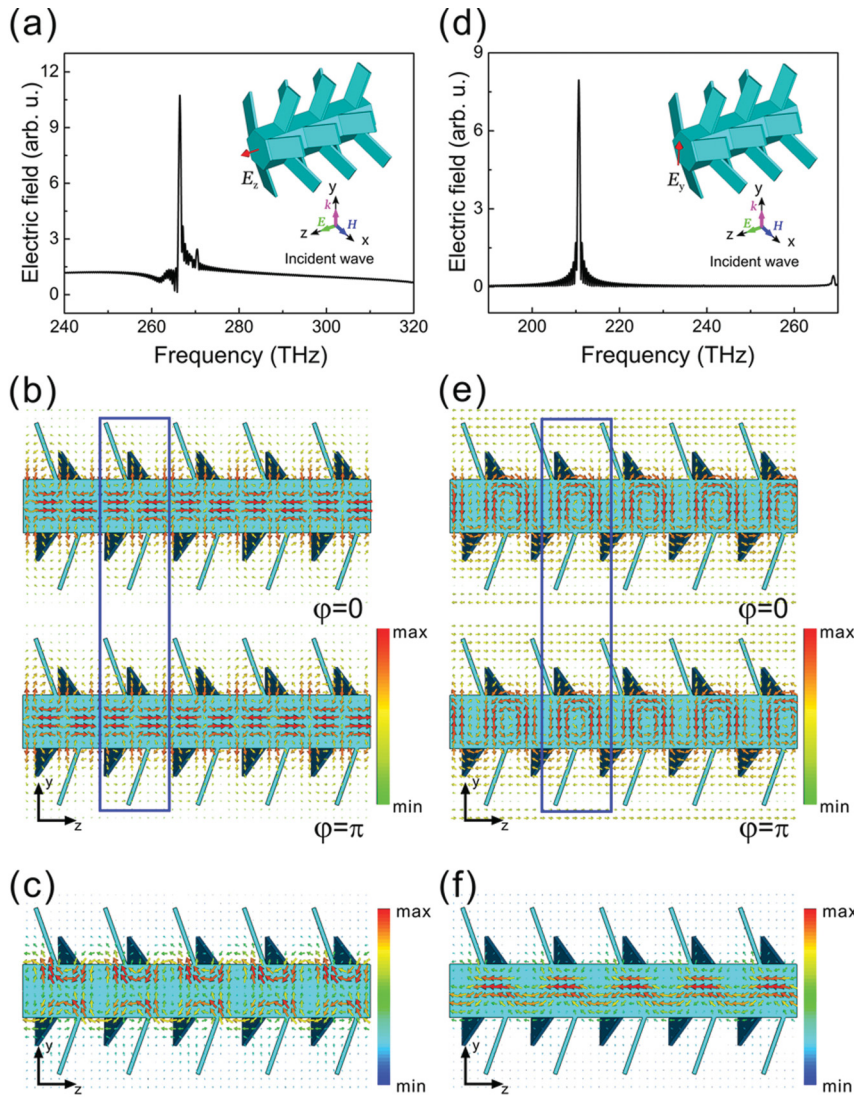
FIG. 6. (Color online) Electromagnetic resonances in the trunk with blades. (a) The resonance of E_z inside the trunk for z-polarized normal incidence. (b) The distribution of the electric field at the resonant frequency. When the phase difference $\phi = 0$ and π, the electric fields in the neighboring regions in the center of the trunk are head-to-head and end-to-end, respectively, as illustrated in the blue box. (c) At the resonance the Poynting vector is zigzag transported near the trunk surface. (d) The other resonance (E_y) detected in the trunk. (e) Plots of the electric field at the resonance on the y-z cross section. When the phase difference $\phi = 0$ and π, the electric field is rotating clockwise and counterclockwise, respectively (see the blue box). (f) Corresponding to the resonance shown in (d) and (e), the Poynting vector zigzag flows along the central axis of the trunk.

exactly from the intersections of the bright and dark emission bands (reentrant corner site), as marked by the arrows in Fig. 5(d).

D. Optical properties of the hierarchical structure

As an effort to explore the application potentials of the novel hierarchical nanostructures, the optical properties of the ZnO trunk decorated with periodically distributed, uniformly angled blades have been numerically studied. The normal incident light is z polarized [inset of Fig. 6(a)]. The electric field inside the trunk is calculated as a function of frequency of the incident light. A resonant electric field has been sensed inside the trunk by a z-polarized detector [Fig. 6(a)]. The resonant frequency depends on the periodicity of the blades on the trunk. At the resonance the spatial distribution of electric field on the y-z cutting plane is plotted in Fig. 6(b), where two rows of circulating vortexes are aligned along the boundaries of the trunk. As illustrated in Fig. 6(b), perpendicular to the trunk, in the y direction, one may identify a pair of oppositely circulating vortexes, which meet in the center of the trunk. Since the electric fields in these two vortexes are circulating in

the opposite directions, the fields at the center of the trunk are parallel to each other. In the same row, the adjacent vortex is rotating in the opposite direction. In Fig. 6(b) two pairs of vortexes are illustrated in the blue box. At the time corresponding to phase difference $\phi = 0$, in the center of the trunk the electric fields contributed by the neighboring vortex pairs are head-to-head; at $\phi = \pi$, the field at the center of the trunk contributed by the neighboring vortex pairs are end-to-end. In this case the energy flux of the electromagnetic wave, characterized by the Poynting vector, is stronger near the boundaries of the trunk, as illustrated in Fig. 6(c). It should be pointed out that the integration of the Poynting vector across the x-y plane does not vanish, indicating that a portion of the incident energy is indeed zigzag transported in the z direction near the trunk surface.

Keeping the incident light z polarized, a y-polarized detector inside the trunk also senses a resonant mode at a different frequency, as shown in Fig. 6(d). For this resonant mode, there exists a row of vortexes of electric field centered in the middle of the trunk, as illustrated in Fig. 6(e). At the time corresponding to $\phi = 0$, the vortex of the electric field is rotating clockwise; at the time corresponding to $\phi = \pi$,

however, the vortex rotates counterclockwise. Meanwhile, the Poynting vector zigzag flows in the center of the trunk in the *z* direction [Fig. 6(f)], and the integration of the Poynting vector across the *x*-*y* plane does not vanish, either. Figure 6 indicates that for normal incidence of light, a portion of the incident energy is coupled into the trunk and is transported in the direction defined by the blades (–*z*). Off the resonant frequencies, no energy flux can be detected in the trunk. Comparing with previous ZnO nanowires without blades,[32] the blades demonstrated here provide the essential boundary conditions for establishing resonance of electromagnetic waves in the trunk at the specific frequencies.

IV. DISCUSSIONS

Despite that the hierarchical nanostructures of ZnO can be generated in the electrochemical system,[26] most of the previous reports provide the examples in vapor growth.[11,12,33] In these cases of the growth of hierarchical nanostructures of ZnO, catalysts were commonly introduced, the growth mechanism was normally attributed to the VLS process,[11,12,33] and the morphology was featured by randomly positioned blades normal to the central trunk. In the VLS mechanism, coherent crystallographic relations between the blades and the trunk do not exist. The hierarchical nanostructures in this article, however, distinctly differ from the previous cases not only in geometrical morphologies, but also more essentially in the underlying growth mechanisms. The accumulation of stacking faults along the [0001] direction of ZnO leads to the repeated polytypism of the WZ and ZB phases with intrinsic (in contrast to the extrinsic catalysts) concave corners across the interfaces of the WZ-ZB phases, which provide preferable sites for nucleation of the paddle blades. Since no catalyst is introduced in the present experiments, the formation of the propellerlike structure is a more inherent process.

Furthermore, our discovery provides an example that in addition to dislocations,[13,14] accumulation of stacking faults can also play an important role in assembling hierarchical structures. The unique hierarchical nanostructure self-assembled may act as a resonant waveguide for light transmission, and hence possess significant potential applications in photonics and energy harvesting.

Finally, we would like to point out that despite our experiment focus on ZnO in this paper, the revealed growth mechanism is not limited to ZnO only. We expect that many semiconductor materials in the II-VI or III-V groups may possess a similar growth behavior. The essential requirement to observe this effect is that the material should have WZ and ZB structures, and these two structures are close in the formation energy, so they are interchangeable and may appear simultaneously. The other requirement is that the material is microscopically polarized, so the nucleation of the blades is selective on a different facet.

ACKNOWLEDGMENTS

*muwang@nju.edu.cn

[1] Z. W. Pan, Z. R. Dai, and Z. L. Wang, Science **291**, 1947 (2001).

[2] Z. L. Wang and J. Song, Science **312**, 242 (2006).

[3] R. Yan, D. Gargas, and P. Yang, Nat. Photonics **3**, 569 (2009).

[4] S. Lal, S. Link, and N. J. Halas, Nat. Photonics **1**, 641 (2007).

[5] D. J. Shu, X. Xiong, Z. W. Wang, Z. Y. Zhang, M. Wang, and N. B. Ming, J. Phys. Chem. C **115**, 31 (2011).

[6] T. Nobis, E. M. Kaidashev, A. Rahm, M. Lorenz, and M. Grundmann, Phys. Rev. Lett. **93**, 103903 (2004).

[7] L. X. Sun, Z. H. Chen, Q. J. Ren, K. Yu, L. H. Bai, W. H. Zhou, H. Xiong, Z. Q. Zhu, and X. C. Shen, Phys. Rev. Lett. **100**, 156403 (2008).

[8] M. Zamfirescu, A. Kavokin, B. Gil, G. Malpuech, and M. Kaliteevski, Phys. Rev. B **65**, 161205(R) (2002).

[9] G. Malpuech, A. Kavokin, A. Di Carlo, and J. J. Baumberg, Phys. Rev. B **65**, 153310 (2002).

[10] R. Johne, D. D. Solnyshkov, and G. Malpuech, Appl. Phys. Lett. **93**, 211105 (2008).

[11] M. H. Huang, Y. Y. Wu, H. Feick, N. Tran, E. Weber, and P. D. Yang, Adv. Mater. **13**, 113 (2001).

[12] P. X. Gao and Z. L. Wang, Appl. Phys. Lett. **84**, 2883 (2004).

[13] R. L. Penn and J. F. Banfield, Science **281**, 969 (1998).

[14] J. D. Eshelby, J. Appl. Phys. **24**, 176 (1953).

[15] M. J. Bierman, Y. K. A. Lau, A. V. Kvit, A. L. Schmitt, and S. Jin, Science **320**, 1060 (2008).

[16] J. Zhu, H. L. Peng, A. F. Marshall, D. M. Bamett, W. D. Nix, and Y. Cui, Nat. Nanotechnol. **3**, 477 (2008).

[17] P. Caroff, K. A. Dick, J. Johansson, M. E. Messing, K. Deppert, and L. Samuelson, Nat. Nanotechnol. **4**, 50 (2009).

[18] H. J. Joyce, J. Wong-Leung, Q. Gao, H. Hoe Tan, and C. Jagadish, Nano Lett. **10**, 908 (2010).

[19] J. Johansson, K. A. Dick, P. Caroff, M. E. Messing, J. Bolinsson, K. Deppert, and L. Samuelson, J. Phys. Chem. C **114**, 3837 (2010).

[20] Ü. Özgür, Y. I. Alivov, C. Liu, A. Teke, M. A. Reshchikov, S. Doğan, V. Avrutin, S. J. Cho, and H. Morkoc, J. Appl. Phys. **98**, 041301 (2005).

[21] Y. Ding, Z. L. Wang, T. J. Sun, and J. S. Qiu, Appl. Phys. Lett. **90**, 153510 (2007).

[22] A. Ashrafi, A. Ueta, A. Avramescu, H. Kumano, I. Suemune, Y. W. Ok, and T. Y. Seong, Appl. Phys. Lett. **76**, 550 (2000).

[23] L. Lazzarini, G. Salviati, F. Fabbri, M. Zha, D. Calestani, A. Zappettini, T. Sekiguchi, and B. Dierre, Acs Nano **3**, 3158 (2009).

[24] A. I. Persson, M. W. Larsson, S. Steinström, B. J. Ohlsson, L. Samuelson, and L. R. Wallenberg, Nat. Mater. **3**, 677 (2004).

[25] Y. F. Yan, G. M. Dalpian, M. M. Al-Jassim, and S.-H. Wei, Phys. Rev. B **70**, 193206 (2004).

[26]T. Liu, S. Wang, Z. L. Shi, G. B. Ma, M. Wang, R. W. Peng, X. P. Hao, and N. B. Ming, Phys. Rev. E **75**, 051606 (2007).

[27]R. B. Saunders, E. McGlynn, and M. O. Henry, Cryst. Growth Des. **11**, 4581 (2011).

[28]N. B. Ming and I. Sunagawa, J. Cryst. Growth **87**, 13 (1988).

[29]M. Willander, O. Nur, Q. Zhao, L. Yang, M. Lorenz, B. Cao, J. Perez, C. Czekalla, G. Zimmermann, M. Grundmann, A. Bakin, A. Behrends, M. Al-Suleiman, A. El-Shaer, A. C. Mofor,

B. Postels, A. Waag, N. Boukos, A. Travlos, H. S. Kwack, J. Guinard, and D. L. S. Dang, Nanotechnology **20**, 332001 (2009).

[30]H. B. Zeng, G. T. Duan, Y. Li, S. K. Yang, X. X. Xu, and W. P. Cai, Adv. Funct. Mater. **20**, 561 (2010).

[31]C.-Y. Yeh, S.-H. Wei, and A. Zunger, Phys. Rev. B **50**, 2715 (1994).

[32]T. Voss, G. T. Svacha, E. Mazur, S. Muller, C. Ronning, D. Konjhodzic, and F. Marlow, Nano Lett. **7**, 3675 (2007).

[33]J. Y. Lao, J. G. Wen, and Z. F. Ren, Nano Lett. **2**, 1287 (2002).